Supporting Information

Trifunctional Fishbone-like PtCo/Ir Enables High-performance Zinc-air Batteries to Drive the Water-splitting Catalysis

Yingjun Sun,[a,b#] Bolong Huang,[c#] Yingjie Li,[a] Yi Xing,[a] Mingchuan Luo,[a] Na Li,[d] Zhonghong Xia,[a] Yingnan Qin,[a,b] Dong Su,[d] Lei Wang[b] and Shaojun Guo[a,e,f]*

[a]*Department of Materials Science & Engineering, College of Engineering, Peking University, Beijing, 100871, China.*
[b]*College of Chemistry and Molecular Engineering, Qingdao University of Science and Technology, Qingdao 266042, China*
[c]*Department of Applied Biology and Chemical Technology, The Hong Kong Polytechnic University, Hung Hom, Kowloon 999077, Hong Kong SAR.*
[d]*Center for Functional Nanomaterials Brookhaven National Laboratory Upton, NY 11973, USA*
[e]*BIC-ESAT, College of Engineering, Peking University, Beijing, 100871, China.*
[f]*Department of Energy and Resources Engineering, College of Engineering, Peking University, Beijing, 100871, China.*

*E-mail: guosj@pku.edu.cn
[#]These authors contributed equally

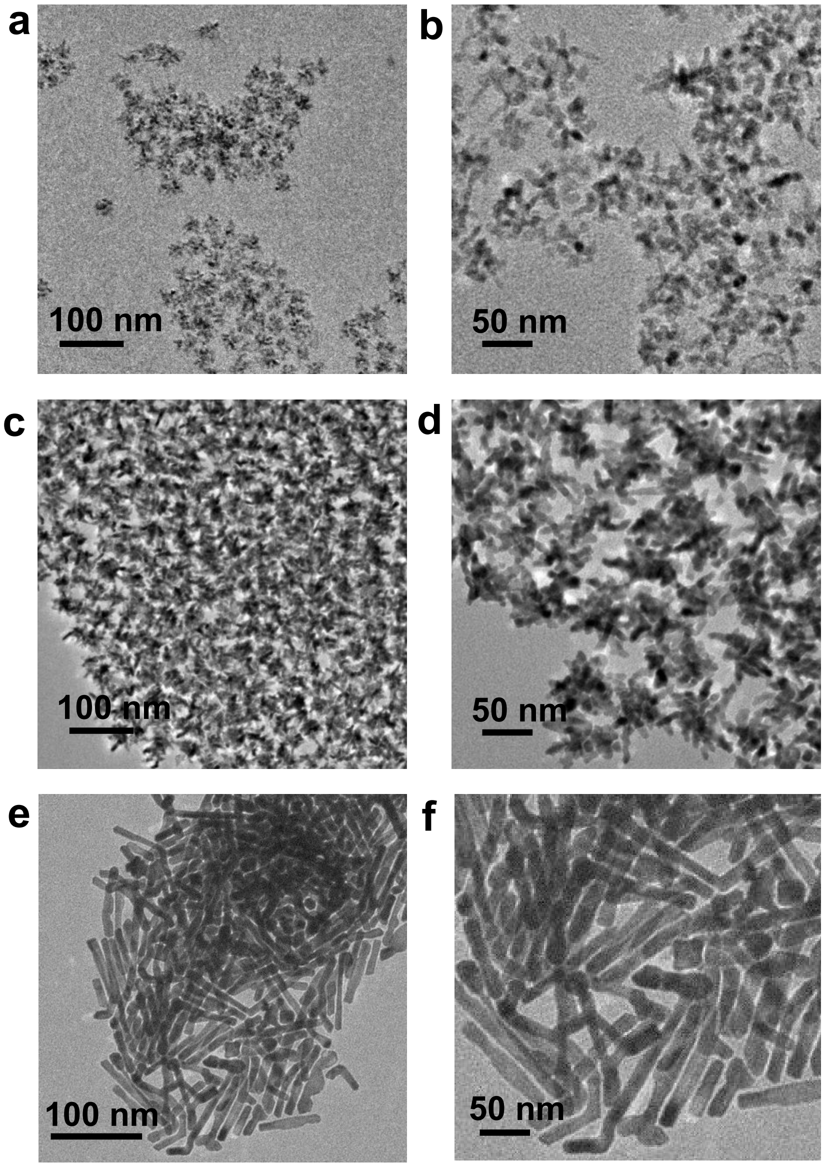

Figure S1. (a, b) Representative TEM images of the products with the same reaction conditions as that of PtCo/Ir FBNWs except the use of 0 mg CTAC, (c, d) 0 mg glucose and (e, f) 0 mg $Co(acac)_3$.

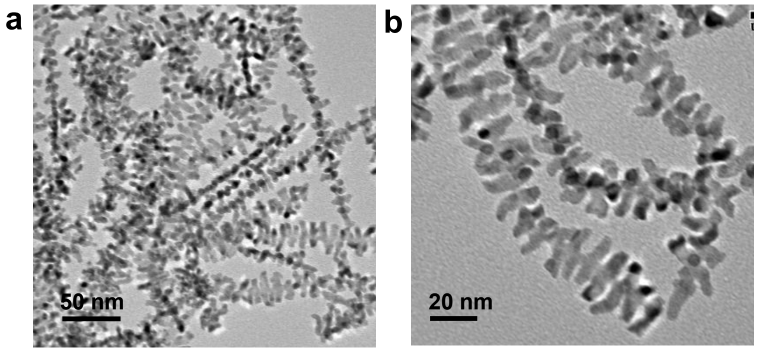

Figure S2. (a) Low- and (b) high-magnification TEM images of PtCo/Ir FBNWs.

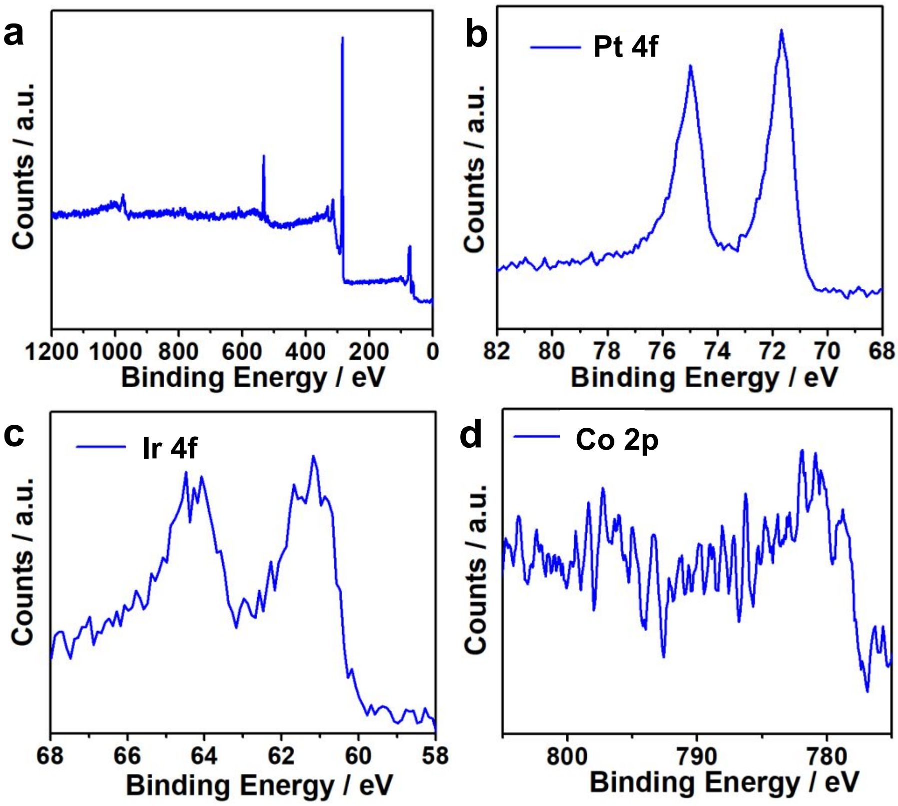

Figure S3. XPS spectra of PtCo/Ir FBNWs. (a) Full survey, (b) Pt 4f, (c) Ir 4f and (d) Co 2p.

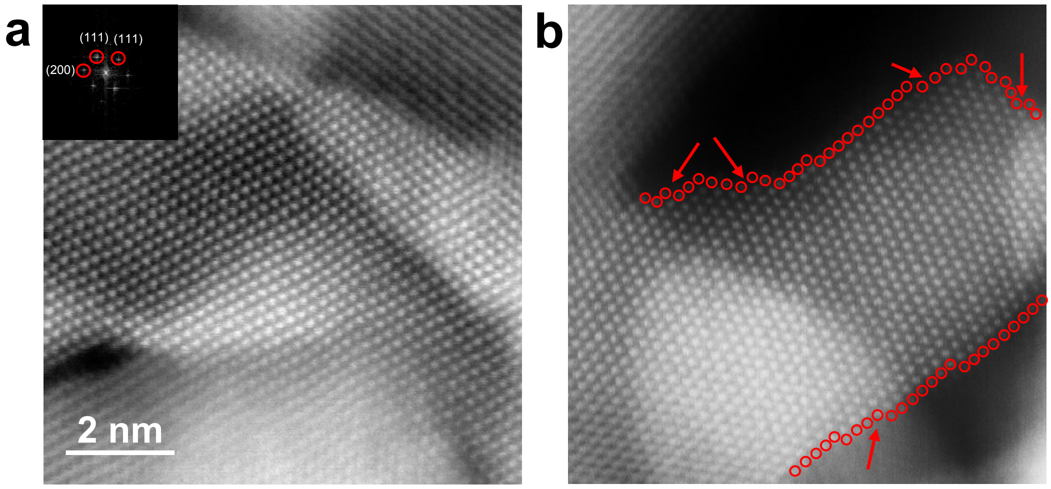

Figure S4. (a) The atomic resolution HAADF-STEM image of PtCo/Ir FBNW. (b) HAADF-STEM image of a single PtCo/Ir FBNW. The inset is FFT pattern of PtCo/Ir FBNW.

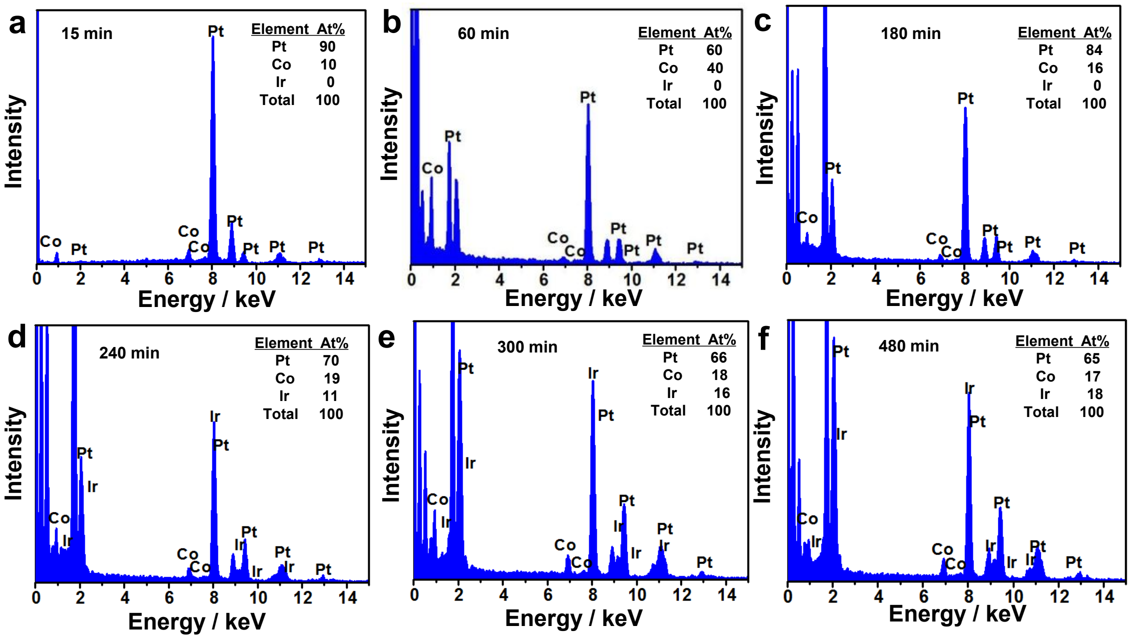

Figure S5. TEM-EDS images of PtCo/Ir FBNWs intermediates collected from (a) 15 min, (b) 60 min, (c) 180 min, (d) 240 min, (e) 300 min and (f) 480 min.

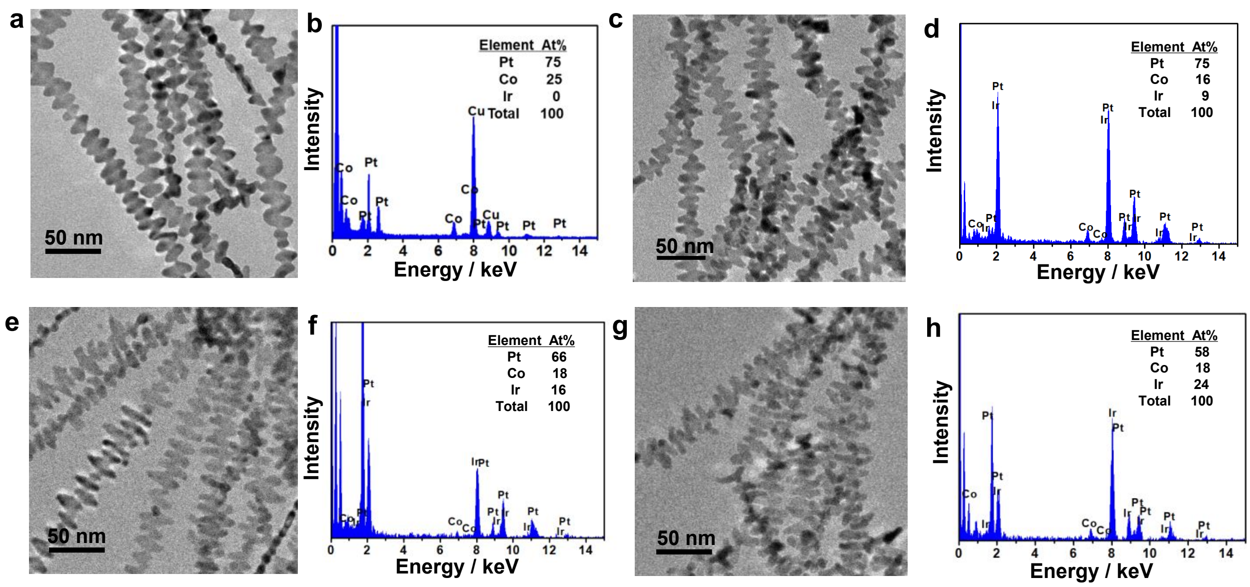

Figure S6. TEM (a, c, e, g) and TEM-EDS (b, d, f, h) images of products with the same reaction conditions as that of PtCo/Ir FBNWs except the use of (a, b) 0 mg, (c, d) 4 mg, (e, f) 8 mg and (g, h) 16 mg $Ir(acac)_3$.

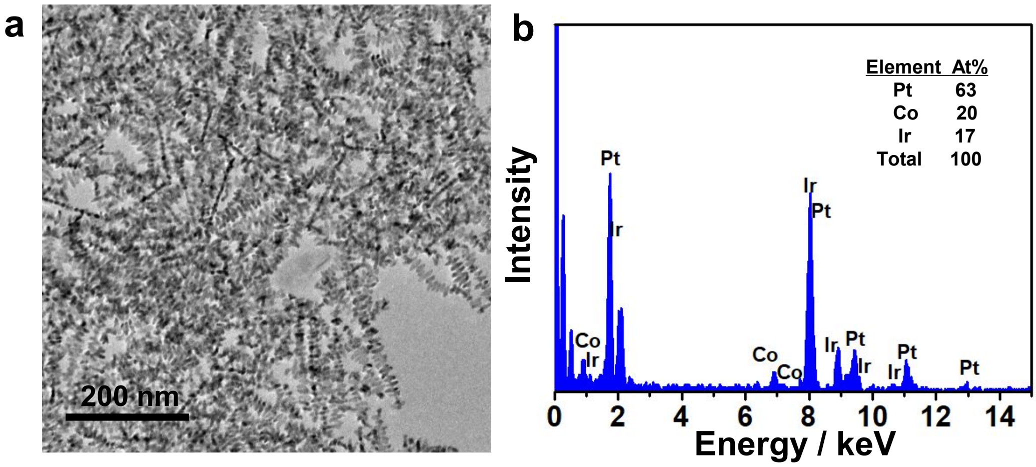

Figure S7. TEM (a) and TEM-EDS images (b) of products with the same reaction condition as that of PtCo/Ir FBNWs except the use of 20 mg Ir(acac)$_3$.

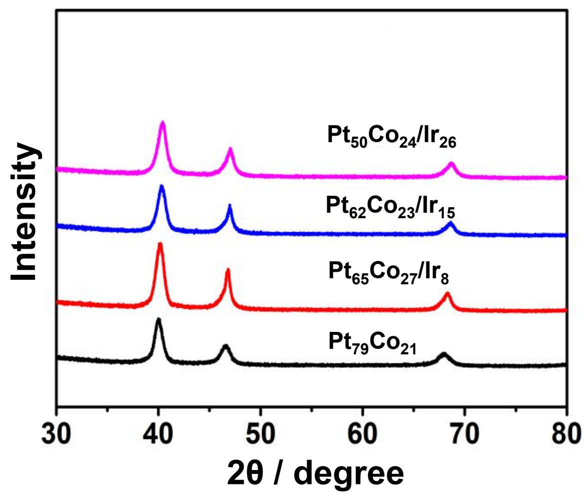

Figure S8. PXRD patterns of rough $Pt_{79}Co_{21}$ NWs, $Pt_{65}Co_{27}/Ir_{8}$ FBNWs, $Pt_{62}Co_{23}/Ir_{15}$ FBNWs and $Pt_{50}Co_{24}/Ir_{26}$ FBNWs.

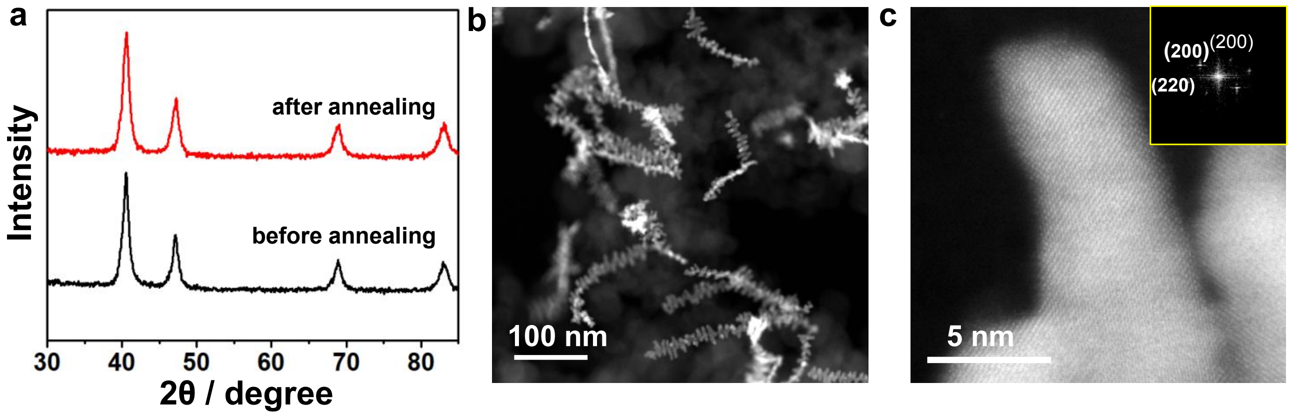

Figure S9. (a) PXRD patterns and (b,c) STEM images of $Pt_{62}Co_{23}/Ir_{15}$ FBNWs/C before and after thermal treatment.

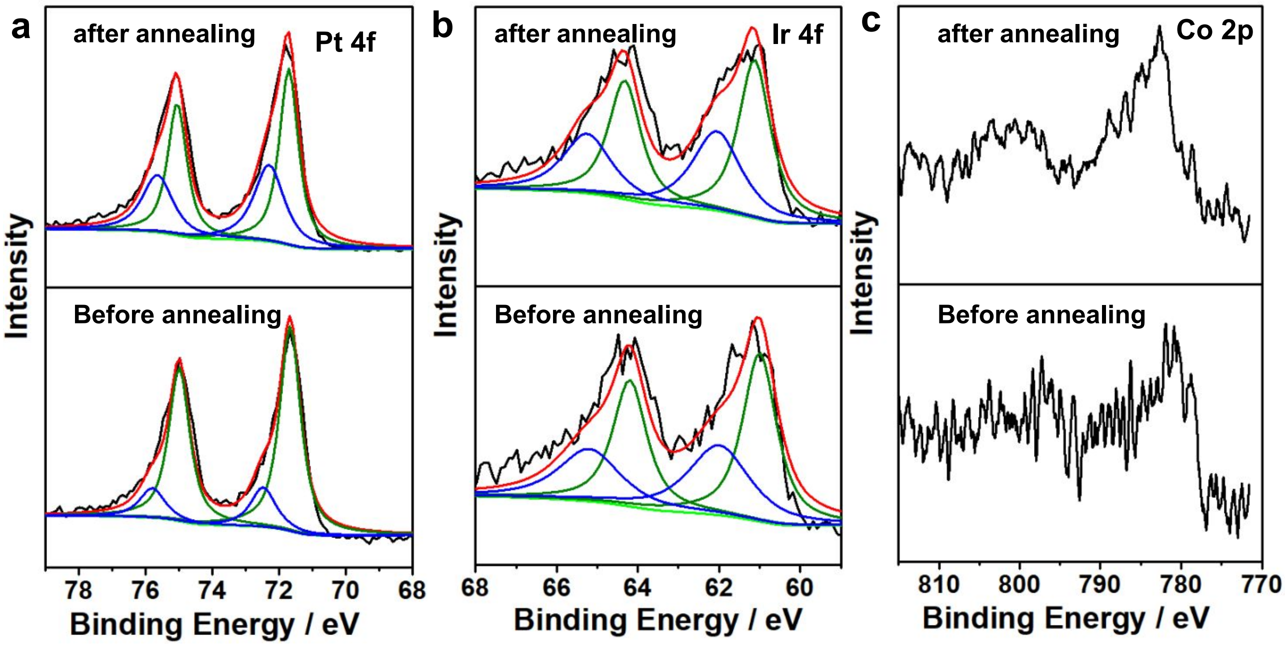

Figure S10. XPS spectra of $Pt_{62}Co_{23}/Ir_{15}$ FBNWs/C. (a) Pt 4f, (b) Ir 4f and (c) Co 2p.

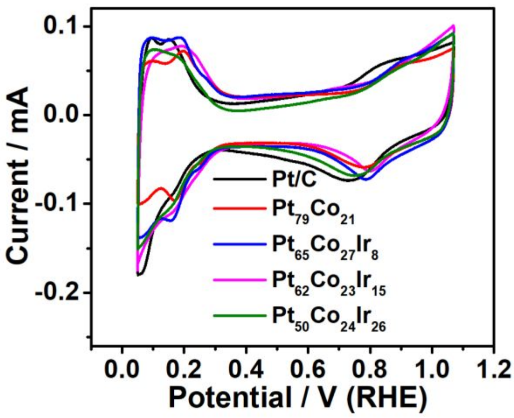

Figure S11. CVs of different catalysts recorded at room temperature in 0.1 M $HClO_4$ solution at a sweep rate of 50 mV/s.

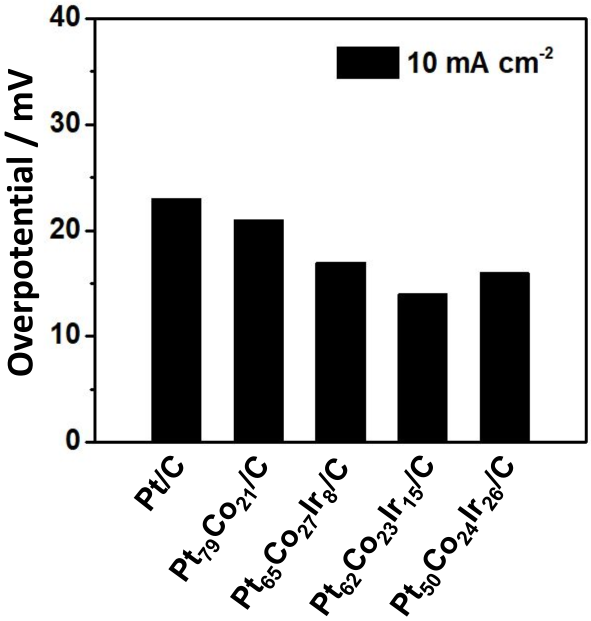

Figure S12. The HER overpotentials of various catalysts at current densities of 10 mA cm^{-2} in 0.1 M $HClO_4$ solution.

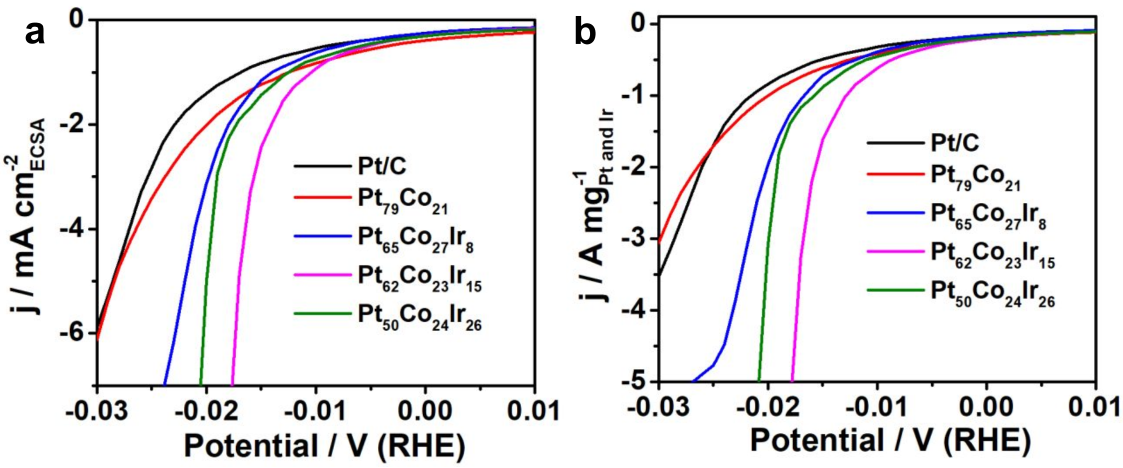

Figure S13. (a) ECSA- and (b) mass- normalized HER polarization curves of different catalysts in 0.1 M $HClO_4$ solution.

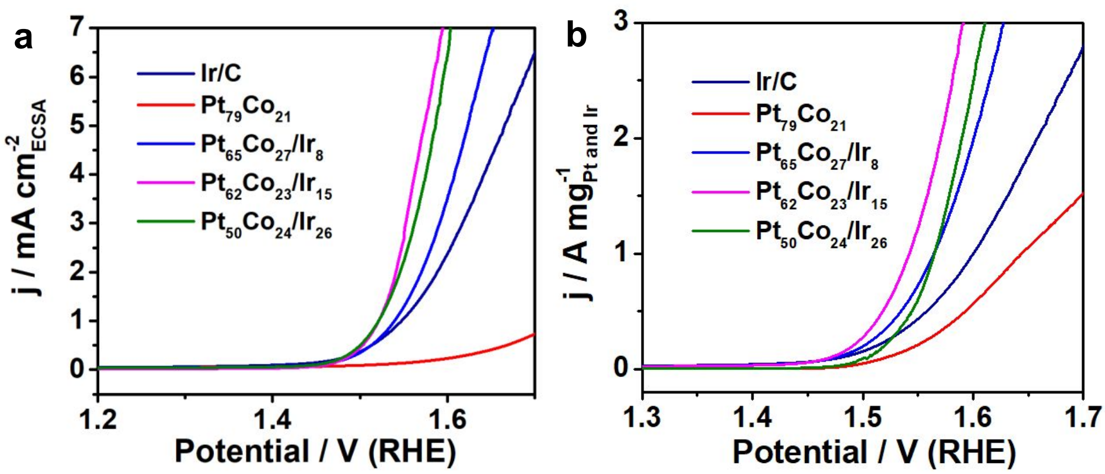

Figure S14. (a) ECSA- and (b) mass- normalized OER polarization curves of different catalysts in 0.1 M $HClO_4$ solution.

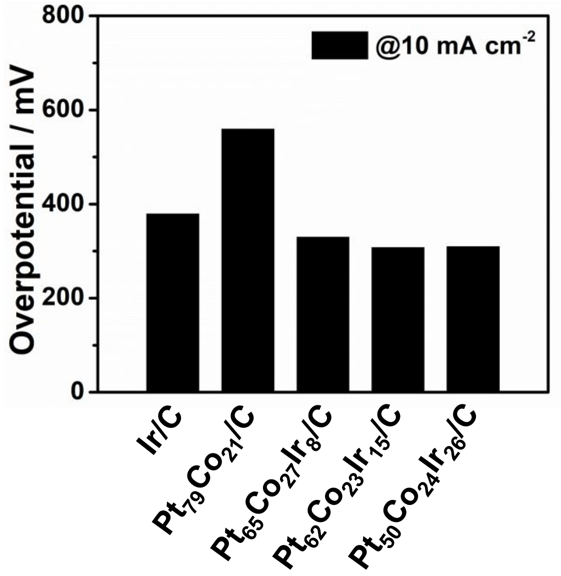

Figure S15. The OER overpotentials of various catalysts at current density of 10 mA cm^{-2} in 0.1 M $HClO_4$ solution.

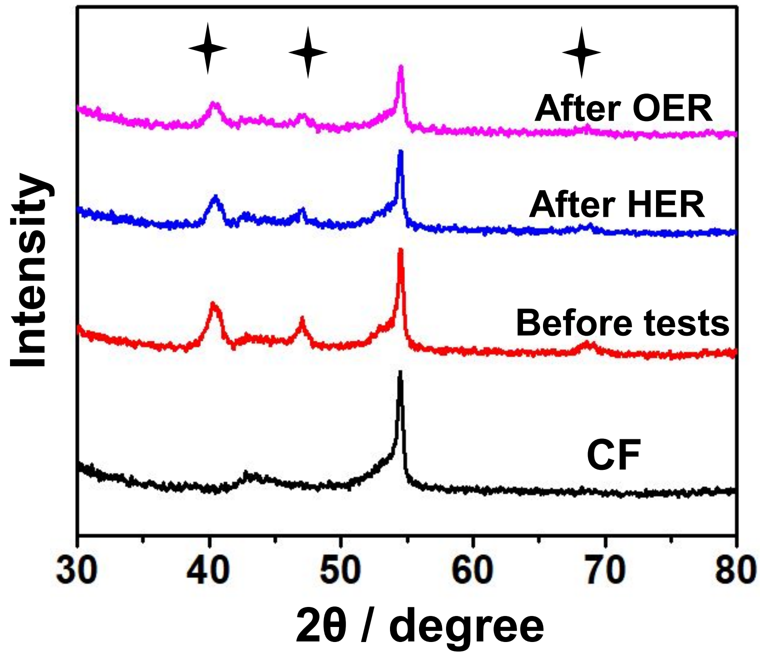

Figure S16. XRD patterns of $Pt_{62}Co_{23}/Ir_{15}$ FBNWs before and after HER and OER tests.

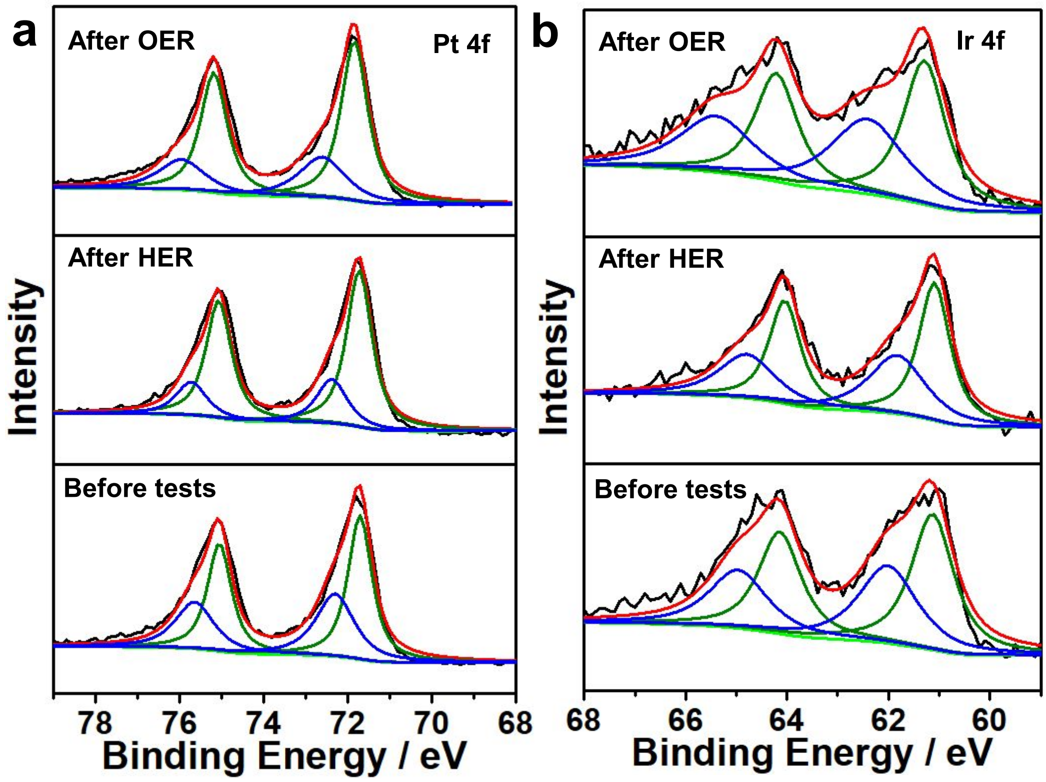

Figure S17. XPS spectra of $Pt_{62}Co_{23}/Ir_{15}$ FBNWs/C. (a) Pt 4f and (b) Ir 4f.

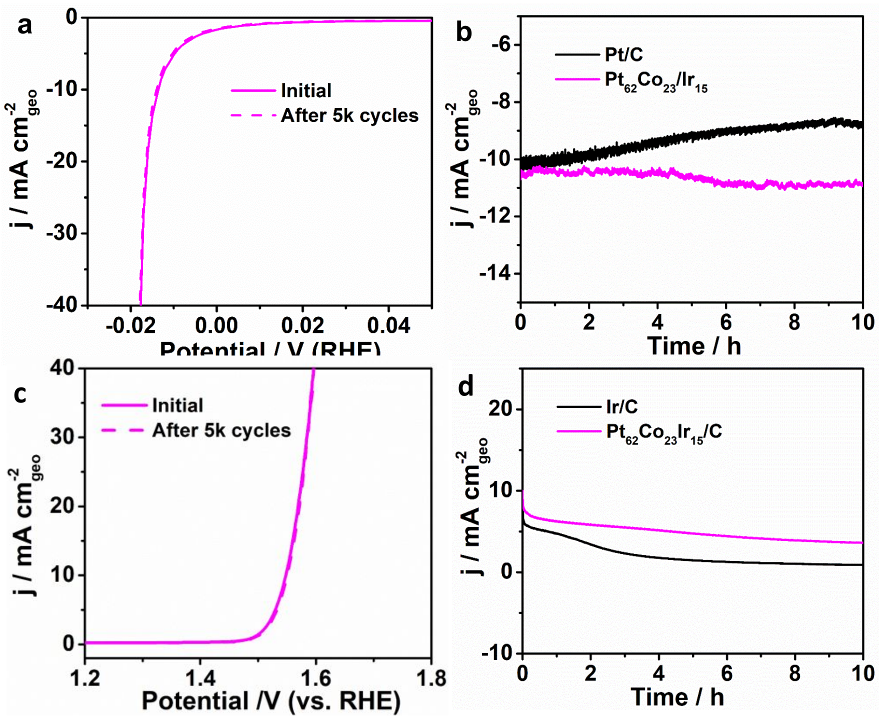

Figure S18. (a) HER and (c) OER polarization curves of $Pt_{62}Co_{23}/Ir_{15}$ FBNWs before and after 5,000 cycles in 0.1 M $HClO_4$ solution. CA tests of Pt/C and $Pt_{62}Co_{23}/Ir_{15}$ FBNWs/C for (b) HER and (d) OER in 0.1 M $HClO_4$ solution.

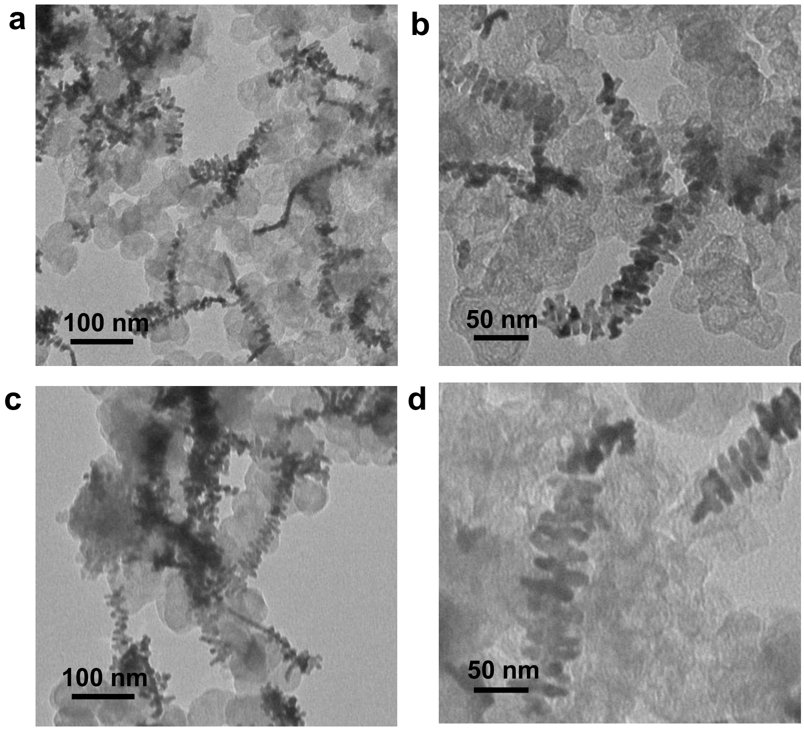

Figure S19. TEM images of $Pt_{62}Co_{23}/Ir_{15}$ FBNWs/C after (a, b) HER and (c, d) OER durability tests.

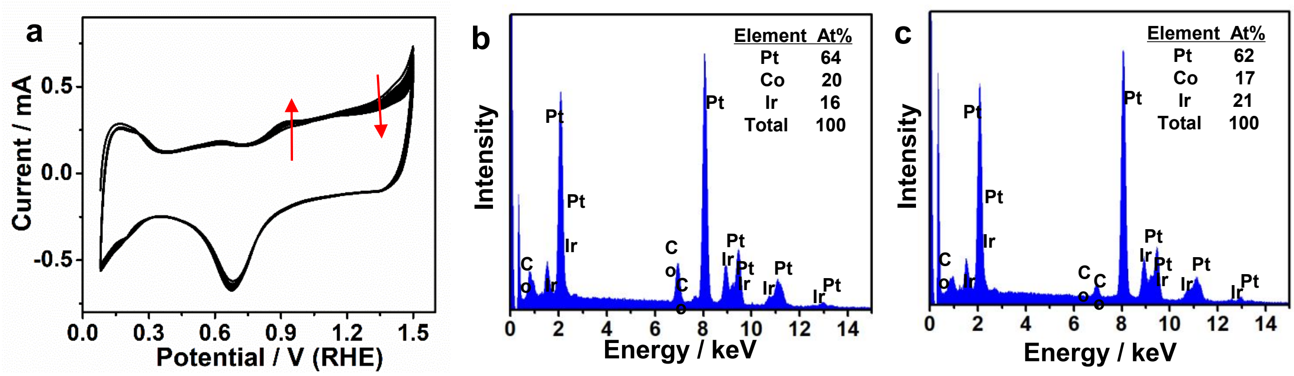

Figure S20. (a) CV activation process of $Pt_{62}Co_{23}/Ir_{15}$ FBNWs/C for OER. TEM-EDS images of $Pt_{62}Co_{23}/Ir_{15}$ FBNWs/C after (b) activation process and (c) durability tests, respectively.

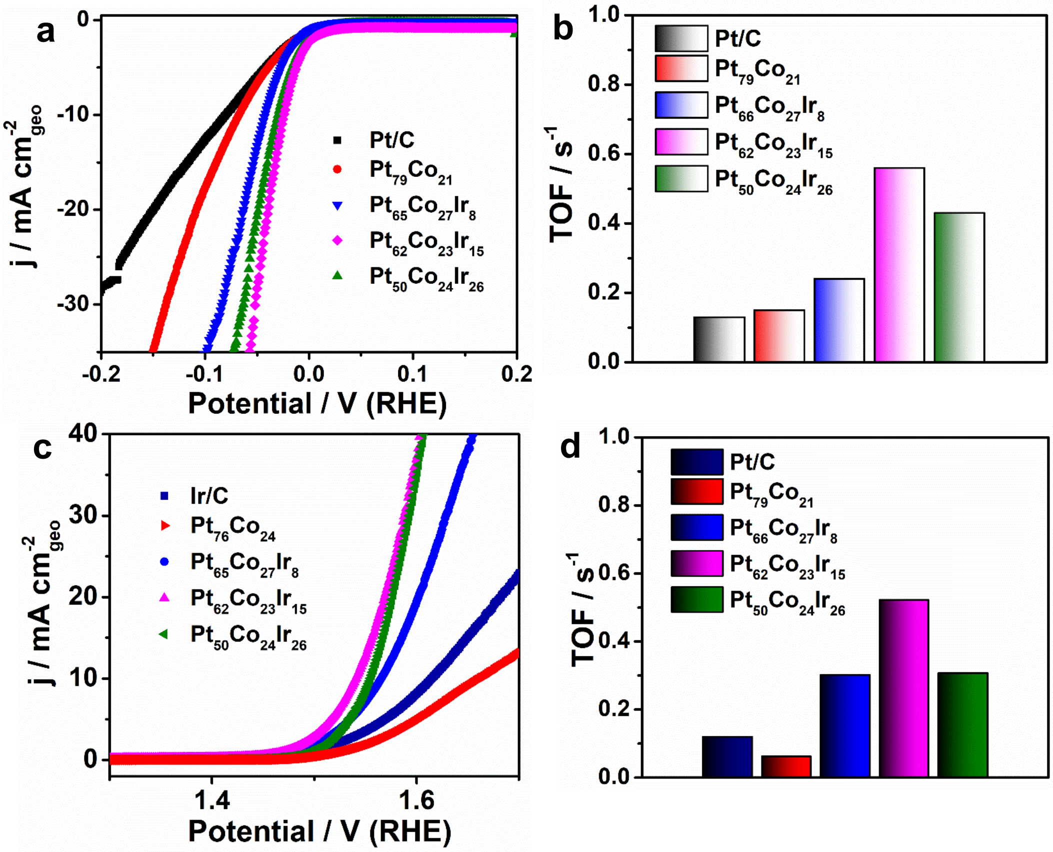

Figure S21. (a) HER polarization curves and (b) TOF values of PtCo/Ir FBNWs/C, PtCo NWs/C and commercial Pt/C in 0.1 M KOH solution. (c) OER polarization curves and (d) TOF values of PtCo/Ir FBNWs/C, PtCo NWs/C and commercial Pt/C in 0.1 M KOH solution.

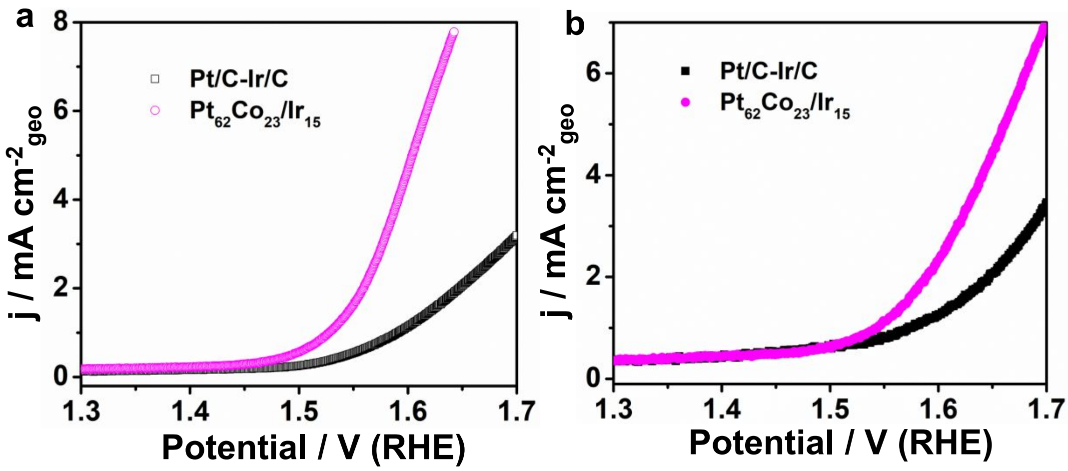

Figure S22. Polarization curves of $Pt_{62}Co_{23}/Ir_{15}$ FBNWs/CFP and Pt/C-Ir/C for overall water-splitting catalysis in (a) 0.1 M KOH solution and (b) 0.1 M PBS solution at a scan rate of 5 mV s^{-1}.

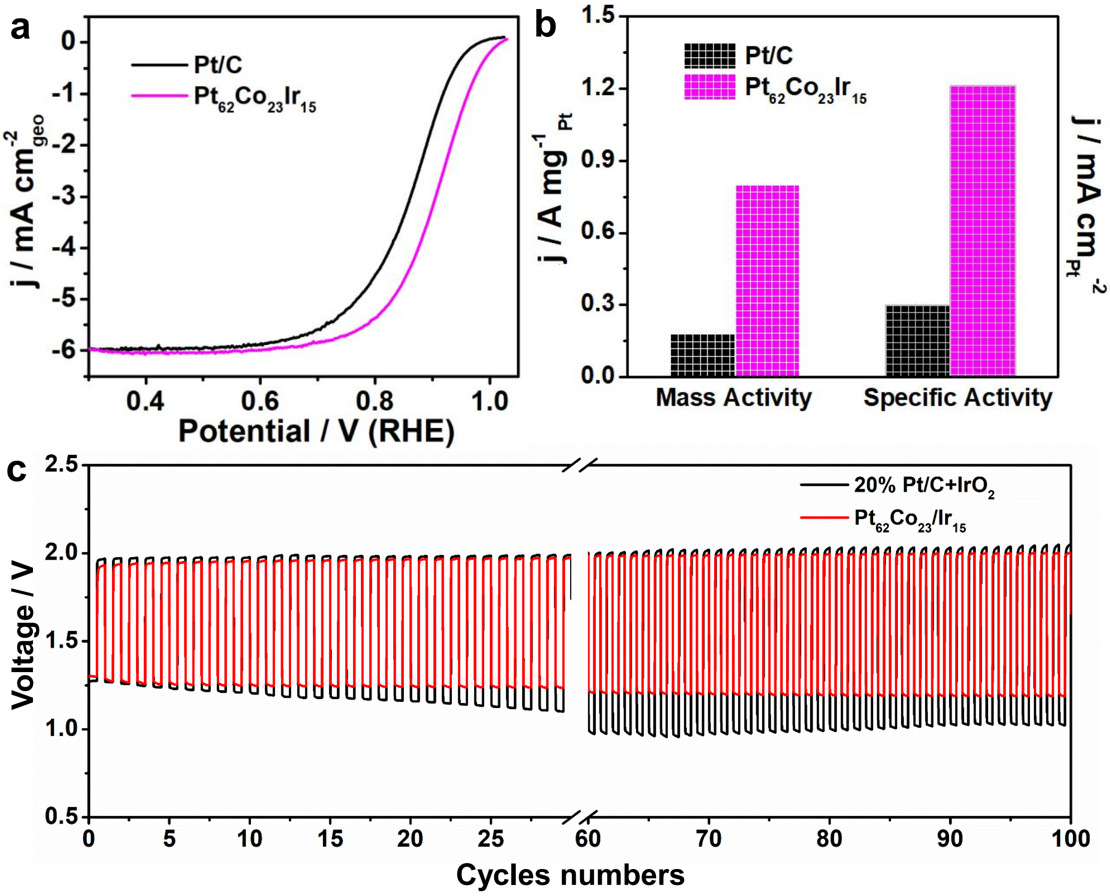

Figure S23. (a) ORR polarization curves and (b) histogram of mass and specific activities of Pt/C and $Pt_{62}Co_{23}/Ir_{15}$ FBNWs/C. (c) Cycling performance of the rechargeable zinc–air batteries based on the $Pt_{62}Co_{23}/Ir_{15}$ FBNWs/C and commercial Pt/C+IrO_2 at 2 mA cm^{-2} with 10 min discharge and 10 min charge.

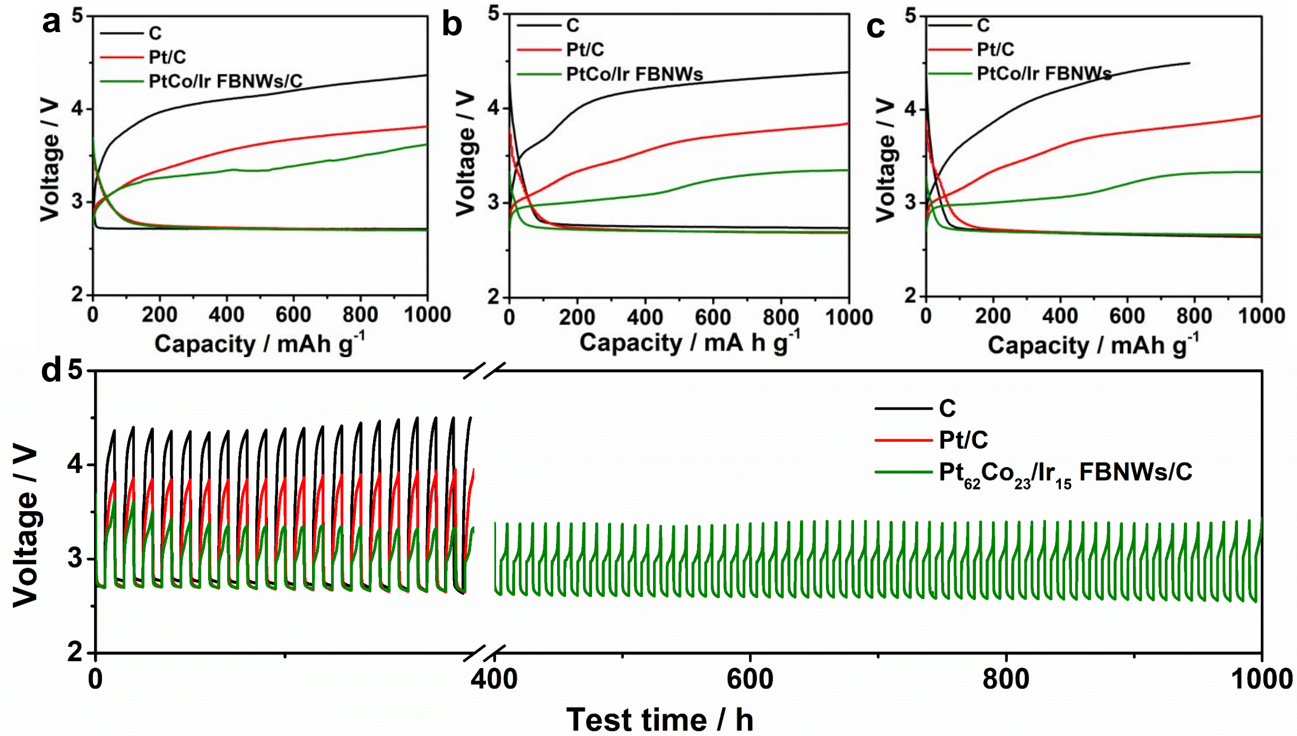

Figure S24. The (a) 1th, (b) 10th and (c) 20th discharge/charge profiles. (d) Cycling performance of the aprotic lithium-O_2 batteries with $Pt_{62}Co_{23}Ir_{15}$ FBNWs/C and carbon as cathodes with a limited capacity of 1000 mAh g^{-1} at the current density of 200 mA g^{-1}.

Electrocatalysts	**Pt loading (μg/cm^2)**	**Ir loading (μg/cm^2)**
Commercial Pt/C	8.7	--
Commercial Ir/C	--	8.2
$Pt_{79}Co_{21}$ NWs/C	8.3	--
$Pt_{65}Co_{27}/Ir_{8}$ FBNWs/C	8.8	1.0
$Pt_{62}Co_{23}/Ir_{15}$ FBNWs/C	8.4	1.98
$Pt_{50}Co_{24}/Ir_{26}$ FBNWs/C	9.2	4.7

Table S1. The Pt or Ir loading of different catalysts on the glass carbon electrode (calculated by ICP-AES).

	Pt	PtO_x	Ir	IrO_x
Before annealing	59.2	40.8	56.1	43.9
After annealing	59.1	40.9	55.9	44.1

Table S2. Proportions of metallic and oxidation states for Pt and Ir before and after 220 ^{o}C thermal annealing.

Catalysts	**ECSA (m^2/g)**
Commercial Pt/C	59.9
Commercial Ir/C	43.7
$Pt_{79}Co_{21}$ NWs/C	49.8
$Pt_{65}Co_{27}/Ir_{8}$ FBNWs/C	62.6
$Pt_{62}Co_{23}/Ir_{15}$ FBNWs/C	66.4
$Pt_{50}Co_{24}/Ir_{26}$ FBNWs/C	61.7

Table S3. ECSA values of various catalysts.

Catalysts	**Ir loading μg/cm^2**	**Electrolyte**	**Current density**	**η/mV**	**References**
$Pt_{62}Co_{23}/Ir_{15}$ FBNWs	1.98	0.1 M $HClO_4$	10 mA/cm^2	308	This work
IrCoNi PHNC	10	0.1 M $HClO_4$	10 mA/cm^2	303	*Adv. Mater.*, **2017**, *29*, 1703798
IrNi oxide	~20	0.1 M $HClO_4$	10 mA/cm^2	310	*J. Am. Chem. Soc.*, **2015**, *137*,13031
$Ir_{0.7}Ru_{0.3}Ox$	60	0.5 M H_2SO_4	100 A/g	270	*Nano Energy* **2017**, *34*, 385
IrW	10.2	0.1 M $HClO_4$	8.1 mA/cm^2	300	*ACS Cent. Sci.*, **2018**, *4*, 1244
Ir WNWs	~31	0.5 M $HClO_4$	10 mA/cm^2	270	*Nanoscale*, **2018**, *10*, 1892
Ir_6Ag_9 NTs	13.3	0.05M H_2SO_4	10 mA/cm^2	296	*Nano Energy* **2019**, *56*, 330
Ir_3Cu	~25	0.1 M $HClO_4$	10 mA/cm^2	298	*ACS Energy Lett.* **2018**, *3*, 2038
IrNi	10.2	0.1 M $HClO_4$	10 mA/cm^2	293	*Small Methods* **2019**, 1900129
Ir/GF	820	0.5 M H_2SO_4	10 mA/cm^2	290	*Nano Energy* **2017**, *40*, 27
Co-IrCu ONC	20	0.1 M $HClO_4$	10 mA/cm^2	293	*Adv. Funct. Mater*. **2017**, *27*, 1604688
$IrNi_{0.56}Fe_{0.82}$	~92	0.5 M $HClO_4$	10 mA/cm^2	284	*J. Mater. Chem. A* **2017**, *5*, 24836

Table S4. Comparisons of OER activities of $Pt_{62}Co_{23}/Ir_{15}$ FBNWs with those of recently reported Ir-based OER catalysis in acidic electrolyte.

	Pt	**PtO_x**	**Ir**	**IrO_x**
Before tests	59.1	40.9	55.9	44.1
After HER	58.9	41.1	55.7	44.3
After OER	61.8	38.2	51.9	48.1

Table S5. Proportions of metallic and oxidation states for Pt and Ir before and after HER and OER electrochemical test.

Catalysts	Ir loading μg/cm^2	Electrolyte	Current density	η/mV	References
$Pt_{62}Co_{23}/Ir_{15}$ FBNWs	8	0.1 M $HClO_4$	10 mA/cm^2	300	This work
IrCoNi PHNC	---	0.5 M H_2SO_4	2 mA/cm^2	330	*Adv.Mater.*, **2017**, *29*, 1703798
IrNi	12.5	0.5 M H_2SO_4	10 mA/cm^2	350	*Adv. Funct. Mater.*,**2017**,*27*,1700886
IrW	30	0.5 M H_2SO_4	10 mA/cm^2	250	*ACS Cent. Sci.*, **2018**, *4*, 1244
Ir/GF	820	0.5 M H_2SO_4	10 mA/cm^2	320	*Nano Energy* **2017**, *40*, 27
Ir WNWs	30.6	0.1 M $HClO_4$	10 mA/cm^2	390	*Nanoscale*, **2018**, *10*, 1892
Ir_6Ag_9 NTs	--	0.5 M H_2SO_4	10 mA/cm^2	320	*Nano Energy* **2019**, *56*, 330
IrNi NFs	30	0.5 M H_2SO_4	10 mA/cm^2	370	*Small Methods* **2019**, 1900129
IrNi NCs	12.5	0.5 M H_2SO_4	10 mA/cm^2	350	*Adv. Funct. Mate*r. **2017**, *27*, 1700886
$IrNi_{0.56}Fe_{0.82}$	200	0.5 M $HClO_4$	10 mA/cm^2	410	*J. Mater. Chem. A* **2017**, *5*, 24836

Table S6. Comparisons of overall water splitting activities of $Pt_{62}Co_{23}/Ir_{15}$ FBNWs with those of recently reported Ir-based overall water splitting catalysis in acidic electrolyte.